Science Advances
AAAS

advances.sciencemag.org/cgi/content/full/6/51/eabc4904/DC1

Supplementary Materials for

An ultrahigh-resolution soft x-ray microscope for quantitative analysis of chemically heterogeneous nanomaterials

David A. Shapiro*, Sergey Babin, Richard S. Celestre, Weilun Chao, Raymond P. Conley, Peter Denes, Bjoern Enders, Pablo Enfedaque, Susan James, John M. Joseph, Harinarayan Krishnan, Stefano Marchesini, Krishna Muriki, Kasra Nowrouzi, Sharon R. Oh, Howard Padmore, Tony Warwick, Lee Yang, Valeriy V. Yashchuk, Young-Sang Yu, Jiangtao Zhao

*Corresponding author. Email: dashapiro@lbl.gov

Published 16 December 2020, *Sci. Adv.* **6**, eabc4904 (2020)
DOI: 10.1126/sciadv.abc4904

This PDF file includes:

VI. RESOLUTION ANALYSIS

The Fourier Ring Correlation (FRC) analysis involves a comparison of two independently measured datasets. In our case, the datasets are measured as part of a single ptychographic scan but are interleaved horizontally. Typical scans are executed with a square grid with scans steps of 40 nanometers in both the horizontal and the vertical directions. When the the goal is to estimate spatial resolution, the horizontal step size is reduced to 20 nanometers so that two normal scans can be extracted such that even steps are used for one scan and odd steps the other. These two ptychographic datasets are submitted to the reconstruction algorithm and the results are use for the FRC analysis. In this way, the FRC is calculated as,

$$FRC(q_i) = \frac{\sum_{q \in q_i} F_1(q) \cdot F_2(q)^*}{\sqrt{\sum_{q \in q_i} F_1^2(q) \cdot \sum_{q \in q_i} F_2^2(q)}} \tag{1}$$

where $F_1(q)$ if the Fourier transform of the image reconstructed using odd scan positions, $F_2(q)$ is that of the image reconstructed using even scan positions and q_i is a spatial frequency bin.

Figure S1 shows ptychographic reconstructions of the same diffraction dataset but with different reconstructed pixel sizes. The pixel size is reduced from the full numerical aperture of the detector by cropping the data as indicated in Figure S2. The images are the amplitude of the sample of Fe3O4 nanoparticles shown in Figure 1. Panels A-D have pixel sizes of 30, 15, 12.5 and 10 nm respectively while the nanoparticles have a mean diameter of 28 nm (center to center distance of 28 nm for two particles). The "ground truth" image is shown in Panel E which uses the full diffraction dataset and has 5 nm pixels. Lineouts of the same region of the images are shown in F and the FRC analysis of the image in B is shown in G. The FRC curve is plotted versus half period spatial frequency (as is common in the literature) and shows a high correlation for image B out to the pixel size of 15 nm. This is likely due to the large diffraction signal that extends to this spatial frequency. Though this would appear to indicate that the achieved resolution is 15 nm, i.e. that 15 nm structures can be resolved, it is clear from the image in B that the 28 nm particles are not clearly visualized. The lineouts shown in F indicate that the oscillations are not all properly reproduced until the pixel size is less than half of the oscillation period (i.e. <14 nm pixels and a 28 nm full period oscillation). This is precisely what would be expected by considering the Shannon-Nyquist sampling theorem which states that the sampling period should be less than half of the oscillation period for faithful reconstruction. A reasonable conclusion to be drawn from this is that, although the FRC can indicate agreement between two

images at a single pixel level, the pixel size is not equivalent to the spatial resolution but rather must be finer than the actual spatial resolution by at least a factor of 2.

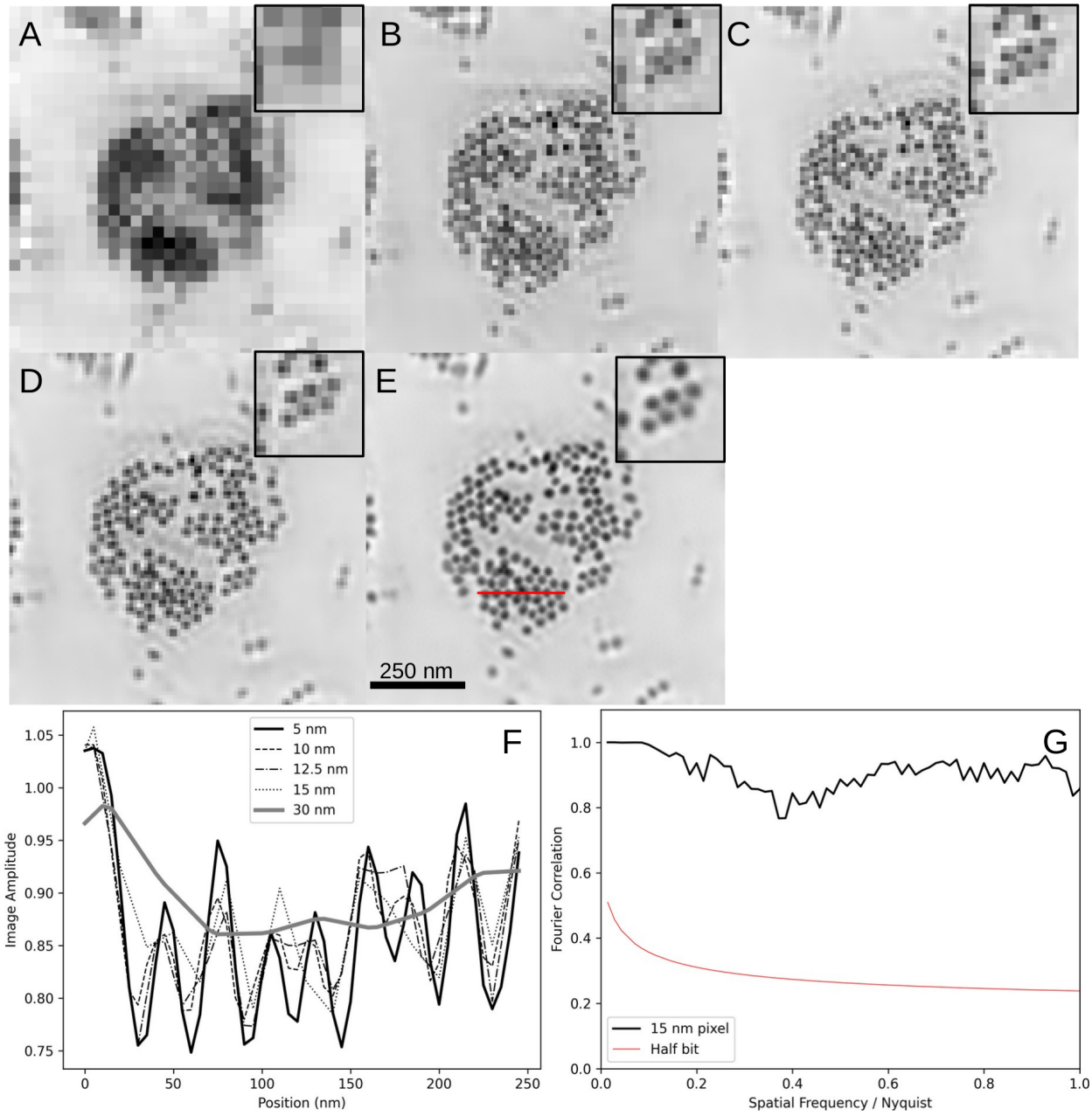

FIG. S1. Achieved spatial resolution as a function of reconstructed pixel size. A-D: images reconstructed from the same diffraction data but cropped to different pixel sizes (30, 15, 12.5 and 10 nm respectively). E: reconstruction of the full diffraction data giving a 5 nm pixel size (the "ground truth" image). F: lineouts from all images along the red line in E. G: Fourier ring correlation curve for the image in B.

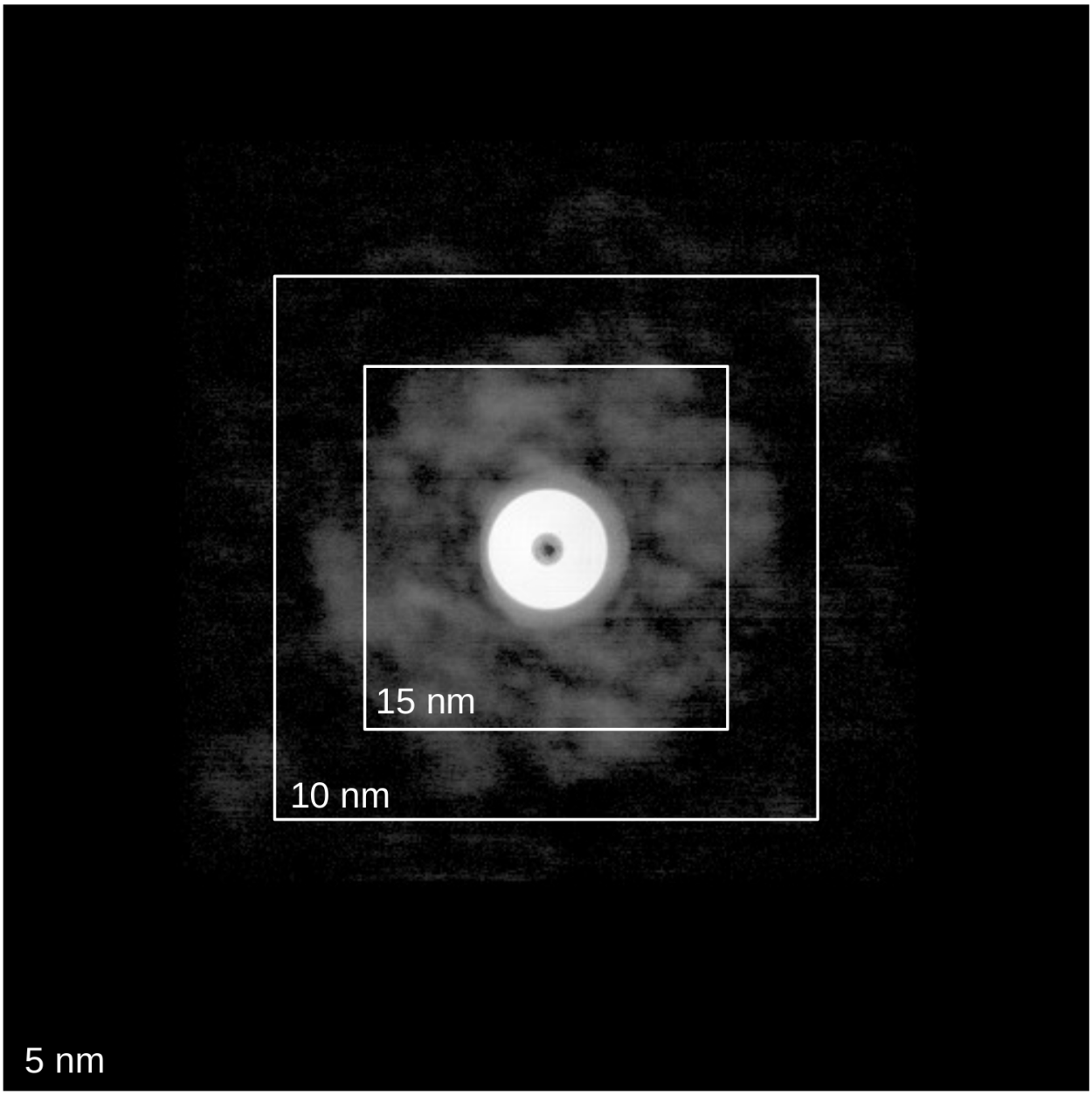

FIG. S2. Single diffraction frame from the dataset used to reconstruct the images in Figure S1. The data were cropped (as indicated by the white squares) in order to achieve different reconstructed pixel sizes.

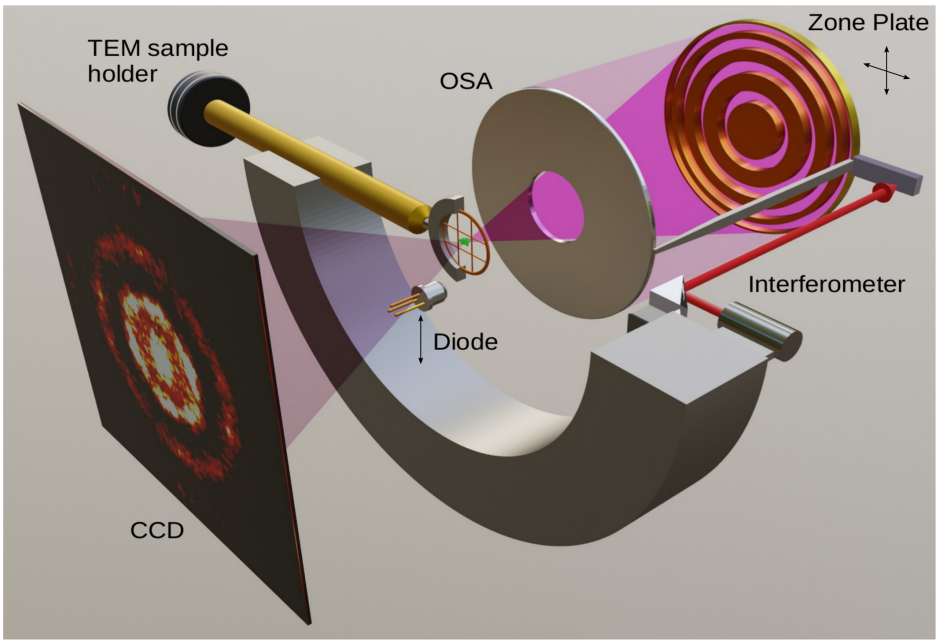

FIG. S3. Conceptual drawing of the microscope. All equipment is mounted to a central cylinder which holds the TEM sample holder manipulator, zone plate scanning mechanism with OSA and interferometer laser heads. The zone plate is scanned relative to this cylinder while the sample is held stationary. A retractable diode detector allows for rapid switching between conventional microscopy and ptychography.

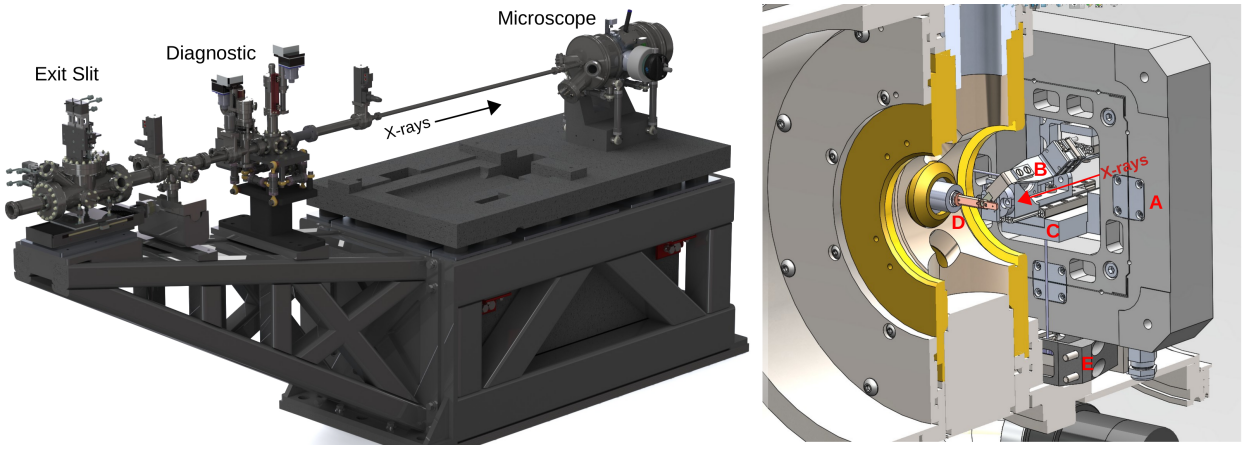

FIG. S4. Left: layout of the microscope support structure including exit slit, beam diagnostic, microscope and vibration damping base. Right: model of the microscope scanning mechanism and sample area. The components are A) XY piezo flexure for zone plate scanning, B) XYZ stage for the order sorting aperture motion, C) zone plate focusing stage, D) tip of the cryogenic sample holder and E) relay mirror for the vertical interferometer beam.

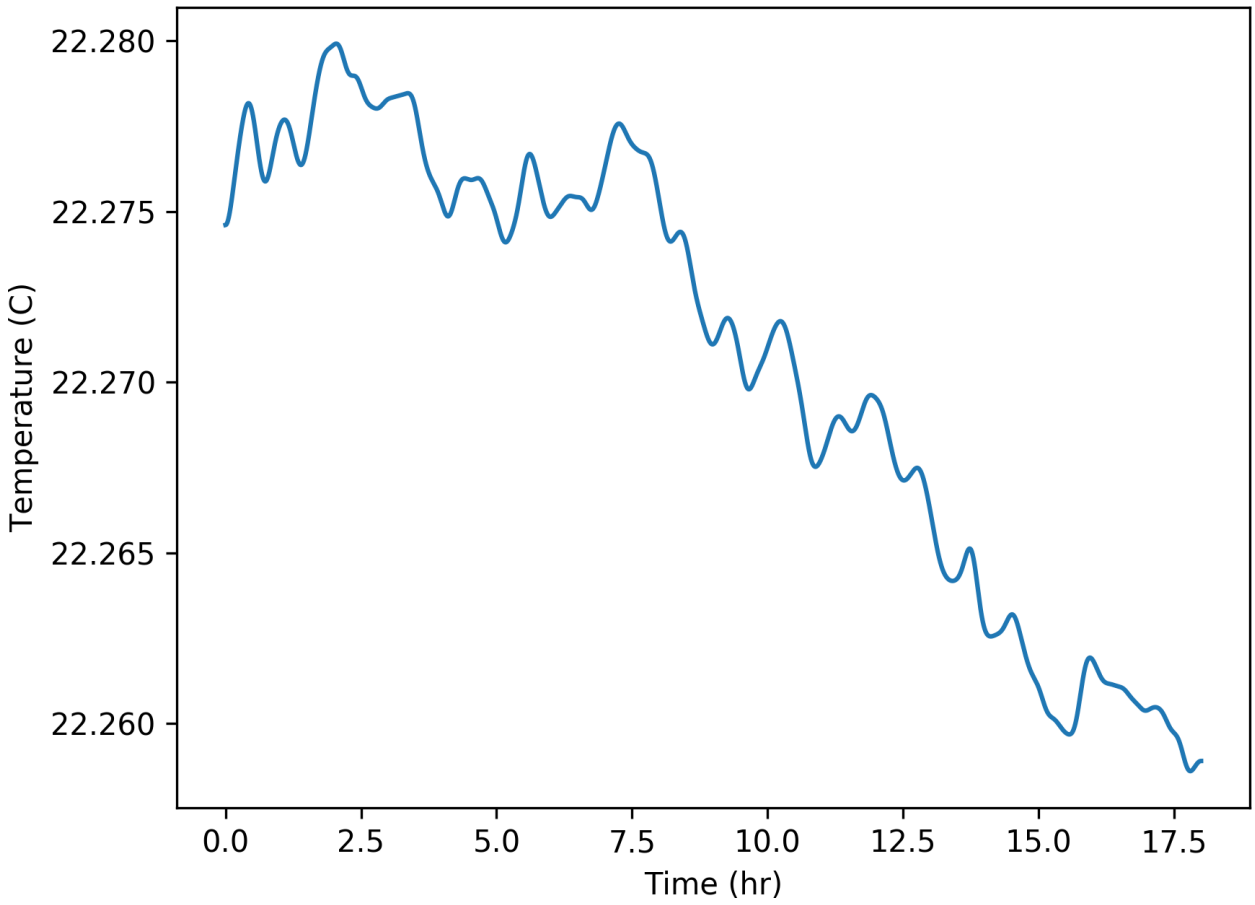

FIG. S5. Temperature measured at the microscope over an 18 hour period. The total temperature variation is below 0.1C.

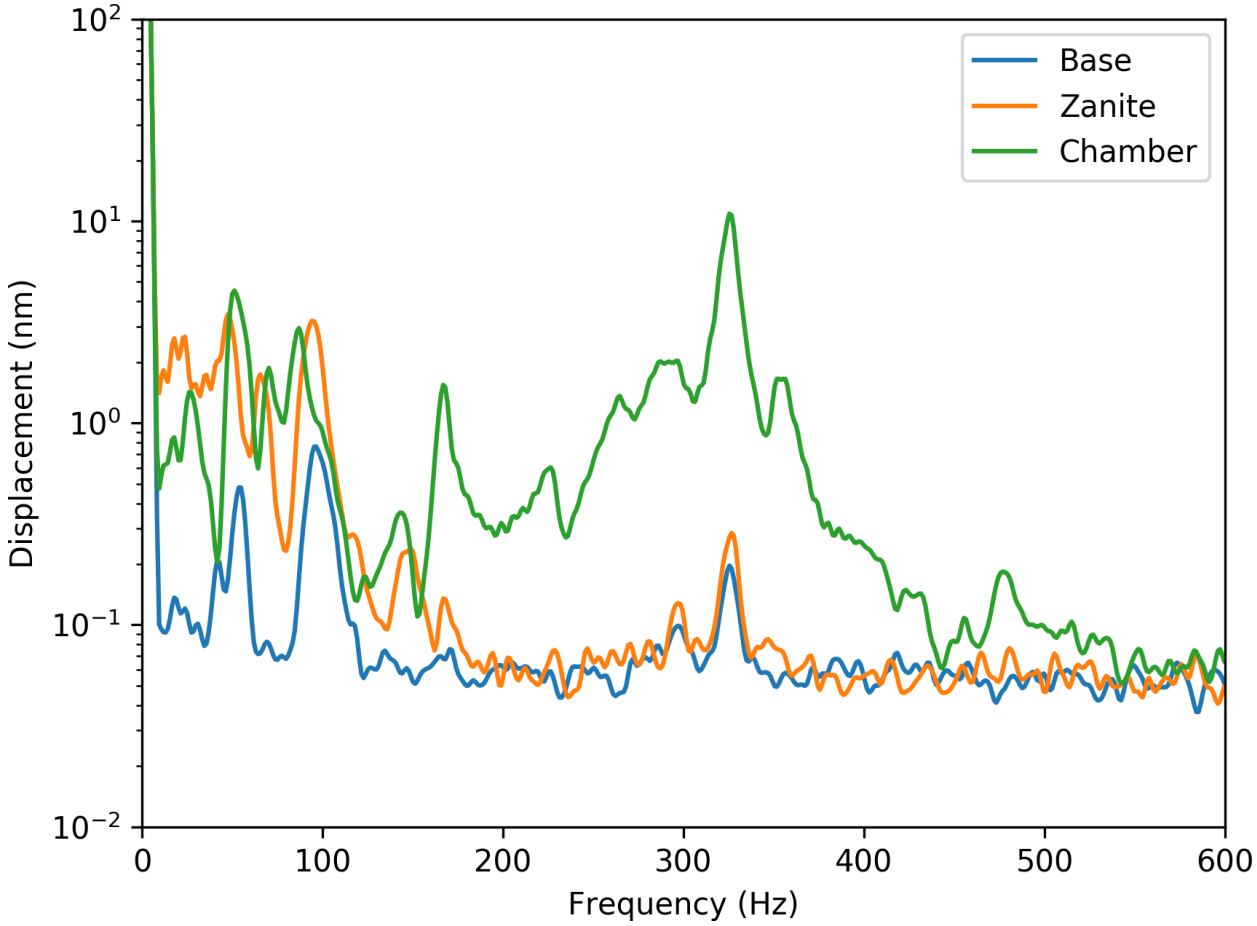

FIG. S6. Displacements measured by the microscope interferometer during impacts to the steel base, the zanite composite table and the microscope chamber. Passive damping between the base and the table reduces the effect of environmental excitation.

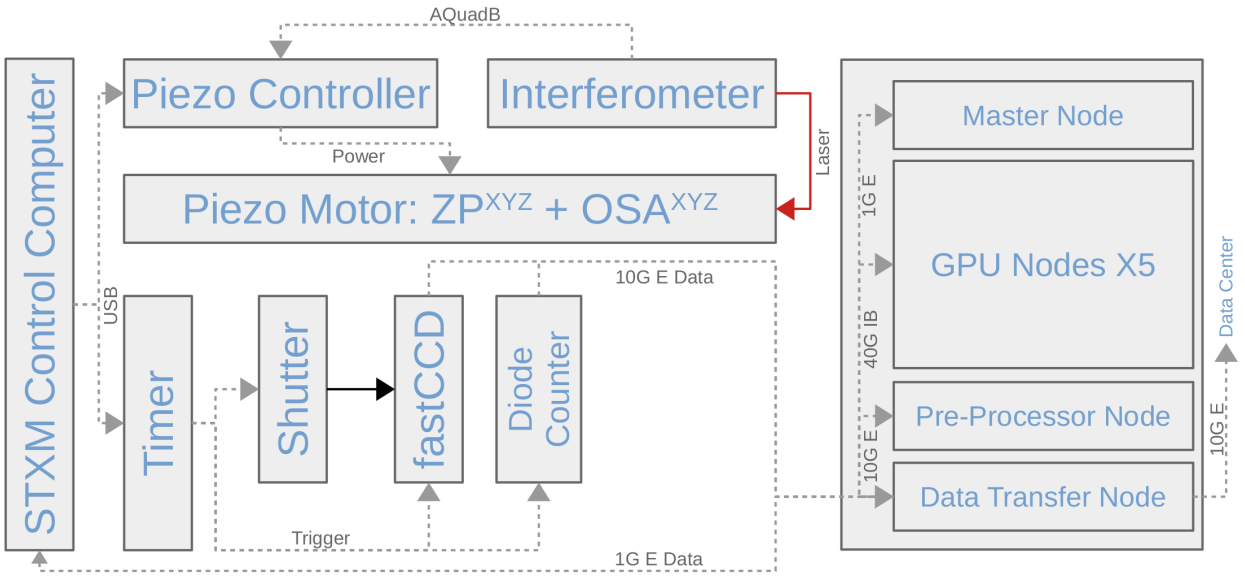

FIG. S7. Schematic of the controls and data flow. A timer triggers the fastCCD or the diode counter while a piezo controller moves the zone plate X-Y stage under interferometric feedback control. All 6 optical motions are scanned simultaneously in X and Y. Data are saved on a remote data transfer node and can be analyzed on local compute nodes and sent to a data center for further analysis, archival and remote user access.

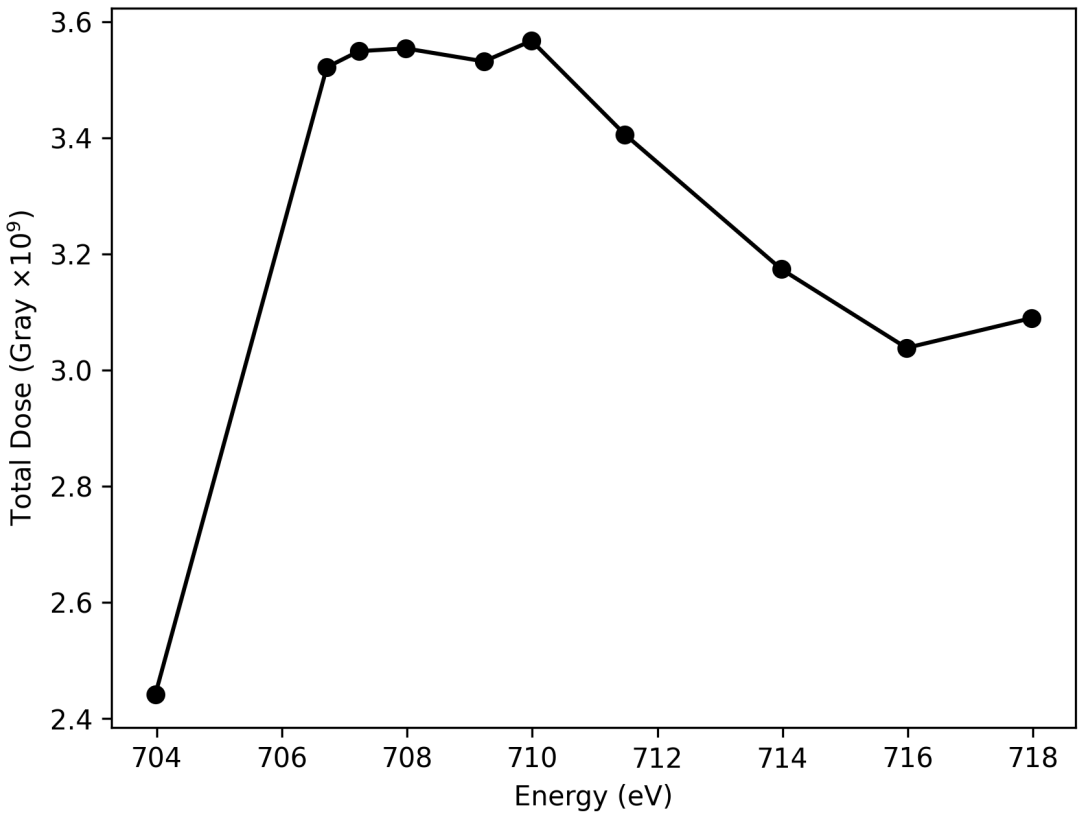

FIG. S8. Estimated dose as a function of energy across the Fe L2 absorption edge. The calculation assumes an incident photon flux of 1×10^8 photons per second in a spot with 55 nm FWHM diameter and a mass density of 3500 kg per cubic meter. The chemical map in Figure 2 used all energy points for a total dose of 3.3×10^{10} Gray while the chemical map in Figure 3 used only the two peak absorption energies (708 and 710 eV) and the pre-edge energy with 50 ms dwell time for a total dose of 9.4×10^9 Gray.

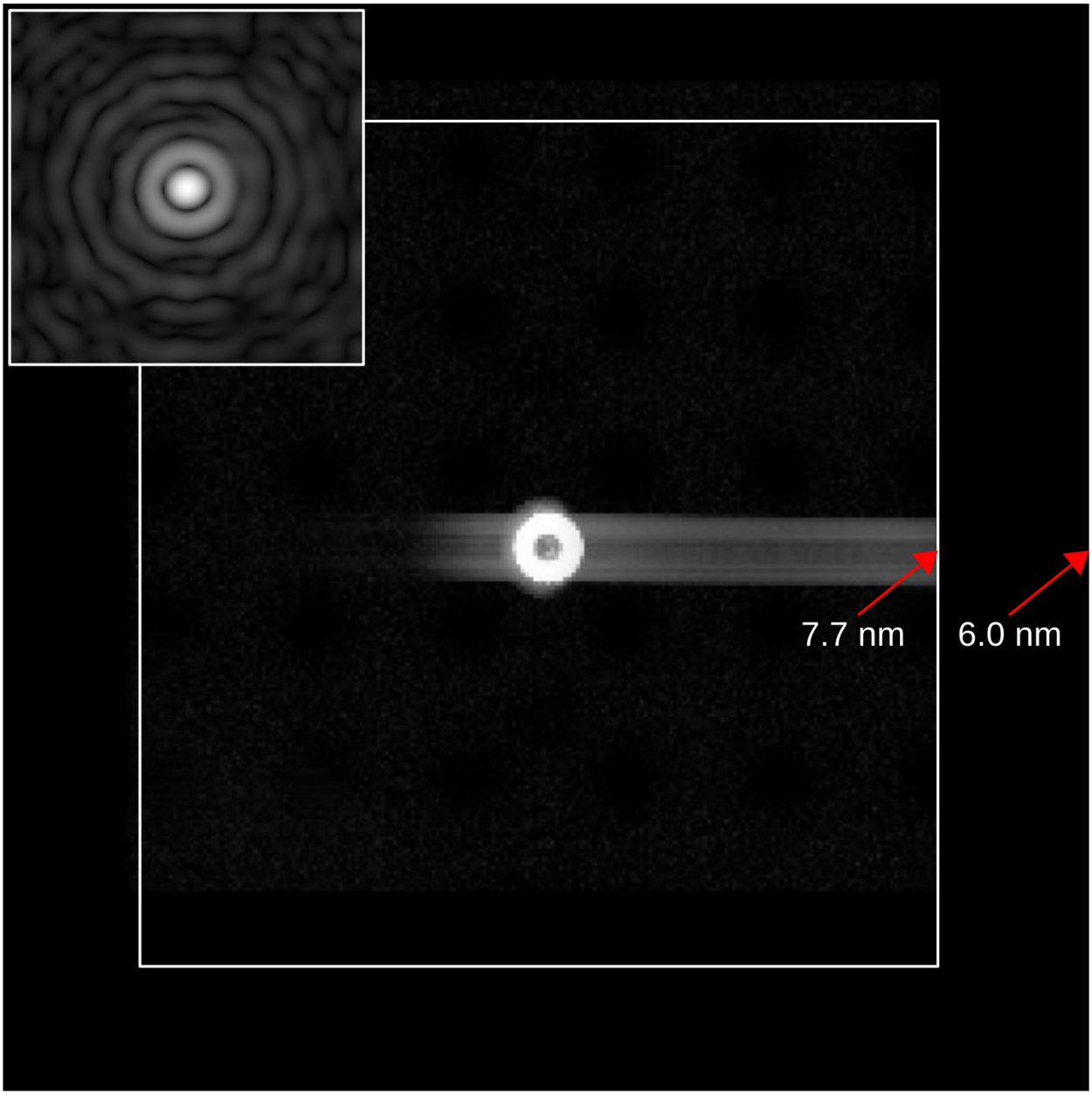

FIG. S9. Average diffraction pattern from the multi-layer structure and reconstructed probe (inset). In both cases the square root of intensity is shown. The large white square represents the coverage of the physical CCD which truncates the diffraction signal at 7.7 nm full period oscillation. The data were padded to 6.0 nm in order to provide a pixel size of 3 nm in the reconstructed image. With this sampling, the illumination envelope covers an area of 768 nm width.